Int. J. Heat Mass Transfer. Vol. 21, pp. 1251–1259
© Pergamon Press Ltd. 1978. Printed in Great Britain

0017-9310/78/0901-1251 $02.00/0

THE EFFECT OF STABLE STRATIFICATION ON THE MOTION IN A ROTATING SPHERICAL ANNULUS

E. J. SHAUGHNESSY
Department of Mechanical Engineering and Materials Science,
Duke University, Durham, NC 27706, U.S.A.

and

R. W. DOUGLASS
Department of Mechanical Engineering, University of Nebraska,
Lincoln, NB 68588, U.S.A.

(*Received* 19 *December* 1977 *and in revised form* 10 *February* 1978)

Abstract—The effects of stable stratification on the steady laminar flow of a viscous fluid in a rotating spherical annulus are investigated. Three rotational configurations are discussed: inner sphere rotating, outer sphere at rest; inner sphere at rest, outer sphere rotating; and both spheres rotating in opposite directions. The calculations include the primary and secondary circulations, the temperature distribution, and the heat-transfer characteristics of the flow. It is shown that the buoyancy forces are effective in reducing the intensity of the secondary circulation, and in one case cause a new circulation pattern to appear.

NOMENCLATURE

C_p, specific heat at constant pressure;
$\tilde{D}$, differential operator;
f_n, angular velocity expansion function;
g_n, stream function expansion function;
g_0, gravitational acceleration;
Gr, Grashof number $g_0\beta(T_2 - T_1)R_2^3/\nu^2$;
h_n, temperature expansion function;
k, thermal conductivity;
P_n, nth order Legendre polynomial;
Pr, Prandtl number $\mu C_p/k$;
q, local heat flux;
Q, total heat flux;
q_c, local conduction heat flux;
Q_c, total conduction heat flux;
r, dimensionless radial coordinate;
$\tilde{r}$, radial coordinate;
Re, Reynolds number $R_2^2\omega_0/\nu$;
R_1, inner sphere radius;
R_2, outer sphere radius;
T, temperature distribution;
T_1, inner sphere temperature;
T_2, outer sphere temperature;
V_r, radial velocity component;
V_θ, latitudinal velocity component;
V_ϕ, azimuthal velocity component;
∇^2, Laplacian operator.

Greek symbols

β, coefficient of volume expansion;
ζ, dimensionless temperature distribution;
η, radius ratio R_1/R_2;
θ, co-latitude;
μ, absolute viscosity;
$\tilde{\mu}$, angular velocity ratio ω_2/ω_1;
ν, kinematic viscosity;
ϕ, azimuthal angle;
ψ, stream function;
ω, rotation function;
ω_0, characteristic time scale;
ω_1, inner sphere angular velocity;
ω_2, outer sphere angular velocity;
Ω, angular velocity function.

1. INTRODUCTION

THE FLOW in a rotating spherical annulus has been extensively studied over the past three decades because of the many geophysical applications. The earliest workers (Howarth [1], Proudman [2], Greenspan [3], and Carrier [4]) were primarily interested in the effects of rotation, and employed methods which were generally of a singular perturbation or boundary-layer character. Their descriptions of the important dynamical mechanisms were subsequently confirmed by Pearson's [5] numerical calculations. In particular, Proudman's [2] cylindrical shear layer was shown to exist not only for nearly rigid rotations but also when one sphere rotates while the other remains at rest. Later Munson [6] did a rather detailed numerical study of the steady flows for all Reynolds numbers up to transition. He also examined the stability of these flows [7].

Progress on the problem of stratified rotating flows in this geometry has followed a similar pattern. Barcilon and Pedlosky [8] constructed a linear theory for cylindrical geometries and clarified the role of the Ekman boundary layer in the limits of weak and strong stable stratification. Later they presented a unified theory [9] which included intermediate stratifications. Their analysis demonstrated that the stably stratified flows could be organized according to the value of the stratification, defined as the product of the

Prandtl number and the stratification parameter. For example, values of the stratification greater than the square root of the Ekman number result in flows for which the Ekman layers are weak or absent. Pedlosky [10] analyzed the stably stratified problem in the spherical annulus using a linearized theory, and pointed out that the effective stratification increases as the equator is approached because the local rotation depends on the latitude. Further work on the stratified problem in cylindrical geometries has been reported by Allen [11, 12], including numerical solutions to the nonlinear problem [13]. The latter work explored the effects of different boundary conditions on flows with strong stable stratification and verified the predictions of the linear theories. Douglass, Munson, and Shaughnessy [14] explored the unstably stratified flows in the rotating spherical annulus using both perturbation and numerical methods. A wide variety of rotational and geometrical configurations were examined, and the unstable stratification was shown to have a profound influence on the meridional circulation. The heat-transfer characteristics of these flows were also discussed.

The work presented here was motivated by the desire to explore the effects of geometry and nonlinearities on the stably stratified problem in the rotating spherical annulus. Solutions are presented for three different configurations: inner sphere rotating, outer sphere at rest; inner sphere at rest, outer sphere rotating; and both spheres rotating, but in opposite directions. The results include the primary and secondary velocity fields, the temperature distribution, and the heat-transfer characteristics of the flow. In all of the flows considered, the stable stratification retards the mechanically driven circulation as the stratification increases. In one flow, however, intermediate stratifications are characterized by an additional secondary circulation which is opposite to the circulation induced by the rotation. The strength of this new secondary motion grows to a value comparable to the primary motion then begins to decay as the stratification increases. An explanation of this phenomenon is given in terms of the spin-up by the mechanical circulation of hot fluid trapped in a buoyancy layer. In all cases considered, the heat transfer across the annulus decreases with increasing stratification, but the precise rate of this decrease varies depending on the rotational configuration.

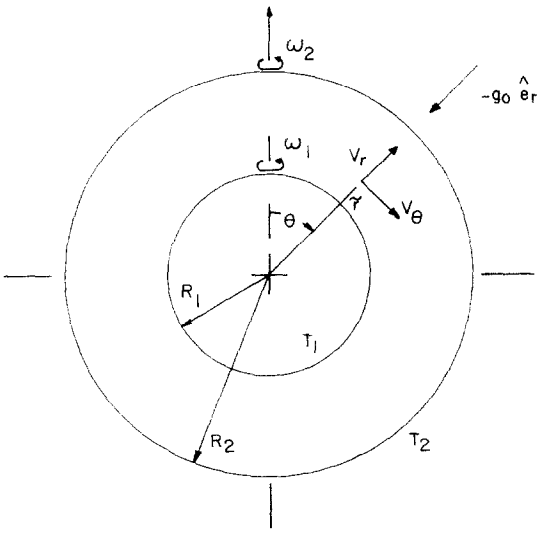

FIG. 1. Flow geometry.

2. ANALYSIS

We consider the motion of a Newtonian fluid in a concentric spherical annulus as shown in Fig. 1. The rigid bounding spheres rotate steadily at rates ω_1 and ω_2 about a common axis. A positive rotation rate denotes clockwise rotation looking in the direction indicated on the polar axis. Both the magnitude and sign of ω_1 and ω_2 are arbitrary; if ω_1 and ω_2 differ in sign, the spheres are counter-rotating. The inner and outer spheres have uniform temperatures T_1 and T_2 respectively, and a uniform gravitational force of magnitude g_0 is assumed to act towards the center of the spheres.

The motion is measured in spherical coordinates (r, θ, ϕ) fixed in space, with (V_r, V_θ, V_ϕ) the corresponding velocity components. The angular coordinate θ is measured from the polar axis; ϕ is the azimuthal angle. The flow is assumed to be steady, independent of ϕ, and symmetric about $\theta = \pi/2$ (the equator). The solutions are valid in the annular region $R_1 \leqslant r \leqslant R_2$, $0 \leqslant \theta \leqslant \pi$, and $0 \leqslant \phi \leqslant 2\pi$ for arbitrary radii R_1 and R_2 of the inner and outer spheres. Due to the assumed symmetries in the problem, the results are presented in the upper portion of a meridian plane only.

The dimensionless equations of motion within the Boussinesq approximation are conveniently formulated in terms of a stream function ψ, an angular velocity function Ω, and a temperature function ζ [14]:

$$\frac{1}{Re}\tilde{D}^2\Omega = \frac{1}{r^2\sin\theta}\left(\frac{\partial\Omega}{\partial r}\frac{\partial\psi}{\partial\theta} - \frac{\partial\Omega}{\partial\theta}\frac{\partial\psi}{\partial r}\right), \tag{1}$$

$$\begin{aligned}\frac{1}{Re}\tilde{D}^4\psi = {} & -(Gr/Re^2)\sin\theta\frac{\partial\zeta}{\partial\theta} \\ & + \frac{1}{r^2\sin\theta}\left\{\frac{2}{r\sin\theta}\left[\Omega\left(\cos\theta r\frac{\partial\Omega}{\partial r} - \sin\theta\frac{\partial\Omega}{\partial\theta}\right)\right.\right. \\ & \left. + \tilde{D}^2\psi\left(\cos\theta r\frac{\partial\psi}{\partial r} - \sin\theta\frac{\partial\psi}{\partial\theta}\right)\right] \\ & \left. + \frac{\partial\psi}{\partial\theta}\frac{\partial}{\partial r}(\tilde{D}^2\psi) - \frac{\partial\psi}{\partial r}\frac{\partial}{\partial\theta}(\tilde{D}^2\psi)\right\},\end{aligned} \tag{2}$$

and

$$\nabla^2\zeta = \frac{RePr}{r^2\sin\theta}\left(\frac{\partial\zeta}{\partial r}\frac{\partial\psi}{\partial\theta} - \frac{\partial\zeta}{\partial\theta}\frac{\partial\psi}{\partial r}\right). \tag{3}$$

Here $Re = R_2^2\omega_0/\nu$ is the Reynolds number, $Gr = g_0\beta(T_2 - T_1)R_2^3/\nu^2$ is the Grashof number, and $Pr = \mu C_p/k$ is the Prandtl number. The Ekman number E is identical to the inverse Reynolds number $1/Re$, while the stratification parameter S is equal to Gr/Re^2. The fluid properties are the kinematic viscosity ν, the absolute viscosity μ, the coefficient of thermal conductivity k,

the specific heat at constant pressure C_p, and the coefficient of thermal expansion β. The non-dimensionalization employs R_2, ω_0^{-1}, and $(T_2 - T_1)$ as the characteristic length, time, and temperature scales. If $\omega_2 = 0$ then $\omega_0 = \omega_1$, otherwise $\omega_0 = \omega_2$.

The dimensional flow variables are defined by the relations

$$V_r = \frac{R_2\omega_0 \dfrac{\partial\psi}{\partial\theta}}{r^2 \sin\theta}$$

$$V_\theta = -\frac{R_2\omega_0 \dfrac{\partial\psi}{\partial r}}{r\sin\theta} \tag{4}$$

$$V_\phi = \frac{R_2\omega_0\Omega}{r\sin\theta}$$

and

$$T = T_1 + (T_2 - T_1)\zeta.$$

The various operators are:

$$\tilde{D}^2 = \frac{\partial^2}{\partial r^2} + \frac{1}{r^2}\left(\frac{\partial^2}{\partial\theta^2} - \cot\theta\frac{\partial}{\partial\theta}\right)$$

$$\tilde{D}^4 = \tilde{D}^2(\tilde{D}^2) \tag{5}$$

and

$$\nabla^2 = \frac{1}{r^2}\left[\frac{\partial}{\partial r}\left(r^2\frac{\partial}{\partial r}\right) + \csc\theta\frac{\partial}{\partial\theta}\left(\sin\theta\frac{\partial}{\partial\theta}\right)\right].$$

The boundary conditions on the flow are that the fluid temperature equals the wall temperature at the spherical boundaries, and that the fluid velocity at the boundaries equals the velocity of the boundaries. In terms of the dimensionless variables these conditions are

$$\zeta(\eta, \theta) = 0, \quad \zeta(1, \theta) = 1$$
$$\psi(\eta, \theta) = \psi(1, \theta) = \frac{\partial\psi}{\partial r}(\eta, \theta) = \frac{\partial\psi}{\partial r}(1, \theta) = 0 \tag{6}$$

and either

$$\Omega(\eta, \theta) = \eta^2 \sin^2\theta, \quad \Omega(1, \theta) = \tilde{\mu}\sin^2\theta (\omega_0 = \omega_1),$$

or

$$\Omega(\eta, \theta) = (\eta^2/\tilde{\mu})\sin^2\theta, \quad \Omega(1, \theta) = \sin^2\theta (\omega_0 = \omega_2).$$

The dimensionless parameters η and $\tilde{\mu}$ which appear in these expressions are the radius ratio of the spheres $\eta = R_1/R_2$, and the angular velocity ratio $\tilde{\mu} = \omega_2/\omega_1$.

The results are represented by plots of the stream function ψ, the temperature function ζ, and the dimensionless rotation ω. The rotation is defined in terms of the angular velocity function by

$$\omega = \frac{\Omega}{r^2\sin^2\theta}. \tag{7}$$

The dimensional value of the azimuthal velocity V_ϕ is

$$V_\phi = R_2\omega_0\omega r\sin\theta. \tag{8}$$

Lines of constant ψ define the secondary flow only. To obtain a complete picture of the motion of a fluid particle, the azimuthal velocity component must also be considered. In a typical case, the particle path is a spiral on the surface of a torus in the spherical annulus.

The temperature distribution in the annulus is represented by plots of the temperature function ζ. Lines of constant ζ are related to the isotherms by equation (4). For example, the line $\zeta = 0.2$ represents a temperature which exceeds the inner cylinder temperature by 20% of the overall temperature difference $(T_2 - T_1)$.

The heat-transfer characteristics of the flow field are represented by the local wall heat flux q, non-dimensionalized by the conduction heat flux q_c. This ratio is evaluated on the inner and outer spheres and plotted as a function of θ. A measure of the overall heat transfer is obtained by integrating the local heat flux over either of the spherical surfaces. This total heat flux Q is given in the form $(Q/Q_c - 1)$, which represents the fractional increase in the total heat transfer attributable to convection. Here Q_c is the total heat transfer predicted by the simple conduction solution. Comparing the values of Q on the inner and outer spheres is a convenient check on the consistency of the numerical technique. For a steady flow in the absence of viscous dissipation these values should be identical.

Numerical solutions to the equations of motion were found using the method of partial spectral expansions [15]. Only the general outline of this procedure will be described here since further details can be found elsewhere. The dependent variables are assumed to have expansions of the form

$$\Omega(r, \theta) = \sin^2\theta \sum_{n=0}^{N} P_n(\theta) f_n(r),$$

$$\psi(r, \theta) = \sin^2\theta \sum_{n=0}^{N} P_n(\theta) g_n(r), \tag{9}$$

and

$$\zeta(r, \theta) = \sum_{n=0}^{N} P_n(\theta) h_n(r).$$

The expansion functions $P_n(\theta)$ are Legendre polynomials of the first kind of order n. The $\sin^2\theta$ factor in the expansions is chosen to simplify the boundary conditions stated in (6). To complete the solution method, the expansions (9) are substituted into the equations of motion, and orthogonality conditions are applied. This reduces the original partial differential equations to ordinary differential equations. The resulting boundary-value problem is solved numerically.

3. RESULTS

Calculations were made for three different cases corresponding to angular velocity ratios $\tilde{\mu} = 0, \infty$, and $-1/3$. The Prandtl and Reynolds numbers are 1 and 10^2 respectively. The results are organized according to the value of the Grashof number which varied between zero (no buoyancy) and 5×10^5. These values lead to stratification parameters in the range $0 \leqslant S \leqslant 50$. Values of S greater than 0.1 represent strong stable stratification according to Barcilon and Pedlosky's [9] criteria. In the discussion that follows the streamlines, isotherms, and local heat flux for each

configuration are described separately. A final section compares the dependence of the total heat flux on the degree of stratification.

(a) *The case* $\tilde{\mu} = 0$

For $\tilde{\mu} = 0$ the inner sphere is rotating steadily while the outer sphere is at rest. The meridional circulation pattern for $Gr = 0$ is counterclockwise, as shown in Fig. 2. As a result of increasing thermal stratification a clockwise circulation pattern appears at the outer edge of the annulus. The first evidence of this new convection cell appears at a Grashof number of 2×10^4,

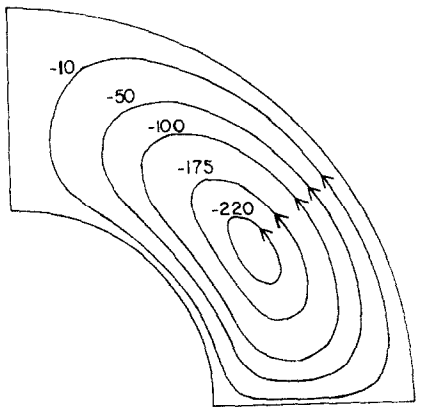

FIG. 2. Streamlines for $\tilde{\mu} = 0$, $Gr = 0$. Values shown are 10^5 times ψ.

which corresponds to a stratification of 2 in the theory of Barcilon and Pedlosky [9]. Below this stratification, all fluid in the annulus circulates counterclockwise. A slight increase in the stratification causes the formation of a very thin layer of fluid of opposite circulation near the outer sphere. This layer extends over all latitudes and initially has a depth of about 1% of the gap. As the Grashof number (and stratification) increase, the new circulation cell increases in strength and size. Figure 3 shows the circulation pattern at a stratification of 45, at which value the clockwise circulation is at its maximum strength. Further increases in the stratification result in continual decreases in the strength of both convection cells.

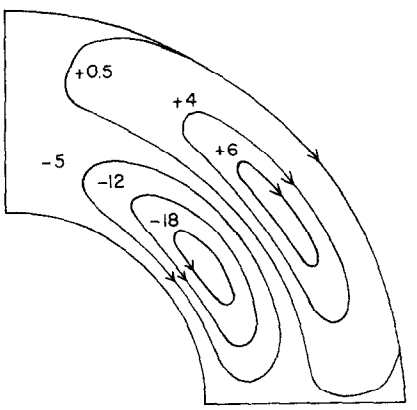

FIG. 3. Streamlines for $\tilde{\mu} = 0$, $Gr = 4.5 \times 10^5$. Values shown are 10^5 times ψ.

This behavior, which has not been described before, appears to be a feature of this particular rotational configuration. With the outer sphere at rest, fluid near this sphere feels a very weak primary motion as evidenced by the angular velocity contours of Fig. 4.

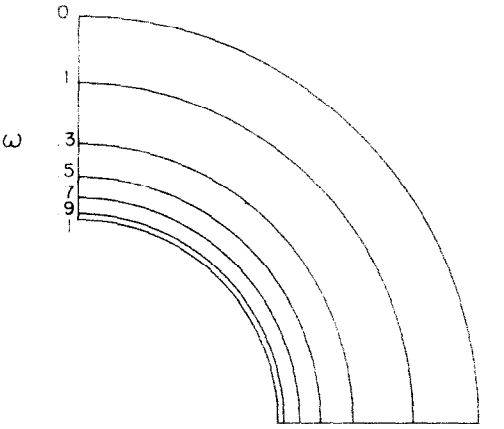

FIG. 4. The ω distribution for $\tilde{\mu} = 0$, $Gr = 4.5 \times 10^5$.

For strong stable stratification, buoyancy forces will tend to resist radial motions of this fluid, causing it to be trapped near the outer sphere. The rotationally driven meridional circulation apparently controls the circulation of this trapped buoyancy layer through simple shear resulting in an opposite circulation. It would be interesting to test this hypothesis by examining the spin-up of this steady flow from a state of stable stratification with the fluid at rest.

Although the buoyancy forces produce a remarkable change in the meridional flow field, the isotherms are relatively unaffected. In the forced convection case ($Gr = 0$) the temperature distribution is similar to the simple conduction solution. The maximum difference between the two distributions is 6% of $(T_2 - T_1)$. As the Grashof number increases to $Gr = 4.5 \times 10^5$ this difference decreases to 0.5% of $(T_2 - T_1)$. In both flows the largest differences occur midway in the gap near the north pole. The local wall heat flux for this flow is shown in Fig. 5 for $Gr = 0$. The values of q/q_c greater than unity on the northern half of the inner sphere reflect the convection of warm fluid to that area by the secondary circulation. As the fluid proceeds along the inner sphere towards the equator its temperature gradually drops, reducing the local heat transfer at the wall. The heat flux falls below the conduction value near the equator because of the deflection of the isotherms by the circulation. Similar reasoning can be used to explain the heat flux values on the outer sphere. As the Grashof number increases, the local heat flux approaches the conduction value and becomes indistinguishable from it for $Gr = 4.5 \times 10^5$.

(b) *The case* $\tilde{\mu} = \infty$

For $\tilde{\mu} = \infty$ the outer sphere rotates steadily while the inner sphere is at rest. The circulation pattern established by the rotation remains essentially unchanged for Grashof numbers as large as 5×10^5.

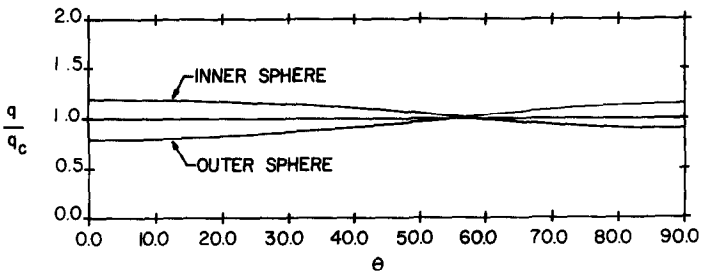

FIG. 5. Local heat flux for $\tilde{\mu} = 0$, $Gr = 0$.

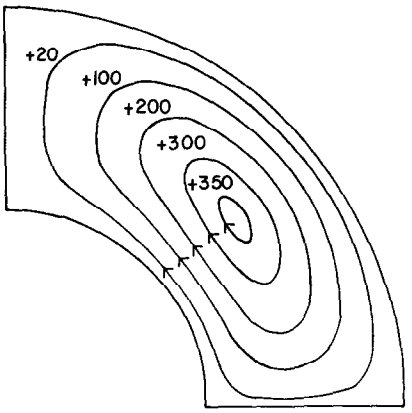

FIG. 6. Streamlines for $\tilde{\mu} = \infty$, $Gr = 0$. Values shown are 10^5 times ψ.

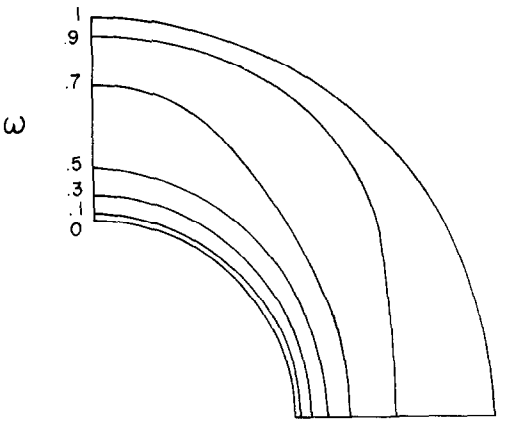

FIG. 8. The ω distribution for $\tilde{\mu} = \infty$, $Gr = 0$.

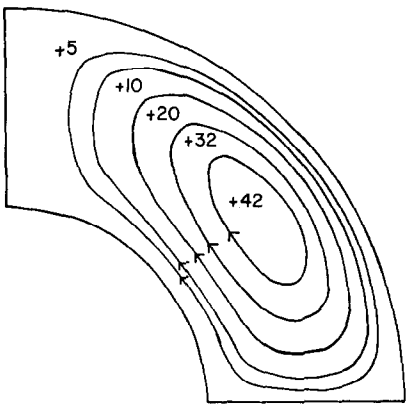

FIG. 7. Streamlines for $\tilde{\mu} = \infty$, $Gr = 2.5 \times 10^5$. Values shown are 10^5 times ψ.

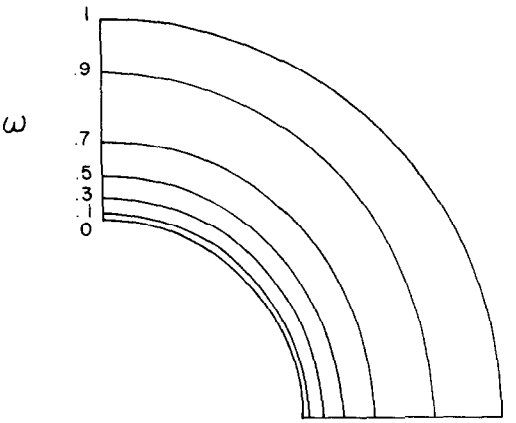

FIG. 9. The ω distribution for $\tilde{\mu} = \infty$, $Gr = 2.5 \times 10^5$.

Figures 6 and 7 show the streamlines for $Gr = 0$ and $Gr = 2.5 \times 10^5$ respectively. Figure 6 may be compared with Pearson's [5] finite difference solution as given by Fig. 3 of his paper. The excellent agreement confirms the basic accuracy of the spectral method used in these calculations. As the stratification increases the intensity of the circulation is reduced but there is little change in the basic circulation pattern. Figure 8 shows the angular velocity distribution in the annulus for $Gr = 0$. The most interesting feature of this distribution is the character of the contours near the equator. We see that Proudman's [2] cylindrical shear layer is present even though the Reynolds number is rather low. Many investigators have exploited this characteristic by constructing simple cylindrical laboratory models of geophysical flows. While this is always valid in the zero buoyancy limit, Fig. 9, which shows the rotation contours for $Gr = 2.5 \times 10^5$, demonstrates that stable stratification destroys this shear layer at low Reynolds numbers.

In the present configuration, as in the previous one, the temperature distribution is similar to that given by the conduction solution. In the forced convection case ($Gr = 0$), the largest difference in the two distributions is 12% of $(T_2 - T_1)$. This is larger than the value found for the previous rotational configuration because the

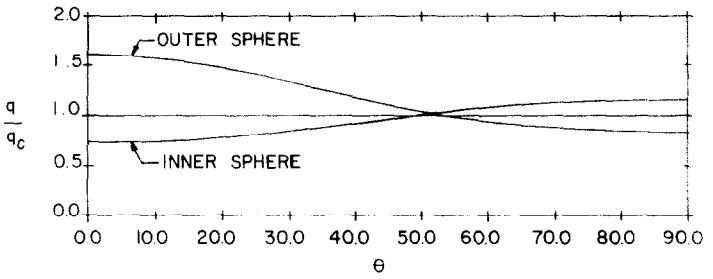

FIG. 10. Local heat flux for $\hat{\mu} = \gamma$, $Gr = 0$.

secondary circulation is stronger. As the Grashof number increases, buoyancy forces retard the circulation and the temperature distribution approaches the conduction distribution. For $Gr = 2.5 \times 10^5$, the difference is down to 1.5%. The local wall heat flux, shown in Fig. 10 for $Gr = 0$ also approaches the conduction heat flux as the Grashof number increases.

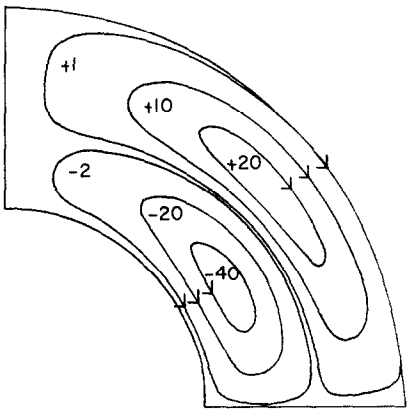

FIG. 11. Streamlines for $\hat{\mu} = -1/3$, $Gr = 0$. Values shown are 10^4 times ψ.

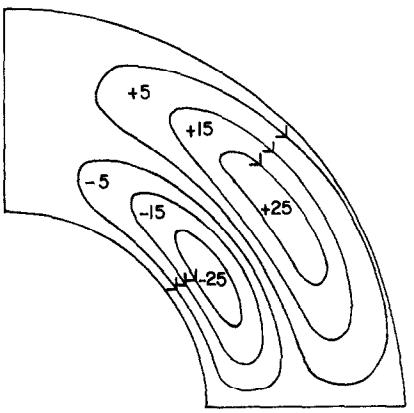

FIG. 12. Streamlines for $\hat{\mu} = -1/3$, $Gr = 1 \times 10^5$. Values shown are 10^4 times ψ.

(c) *The case* $\hat{\mu} = -1/3$

In the last configuration studied, the inner sphere rotates three times as fast as the outer sphere and in the opposite direction. The shear forces established by the differential rotation act in opposite directions at each boundary, resulting in a secondary motion consisting of a pair of counter-rotating eddies. This circulation pattern is illustrated in Fig. 11 for $Gr = 0$, and in Fig. 12 for $Gr = 1 \times 10^5$. In comparison to the previous configurations, the buoyancy forces are not as effective in retarding the circulation. The clockwise motion is actually enhanced by the buoyancy forces for Grashof numbers less than 3×10^5, which is the largest value for which calculations were made. The buoyancy forces do retard the counterclockwise circulation but to a lesser degree than seen earlier. The angular velocity distribution for $Gr = 1 \times 10^5$ is shown in Fig. 13.

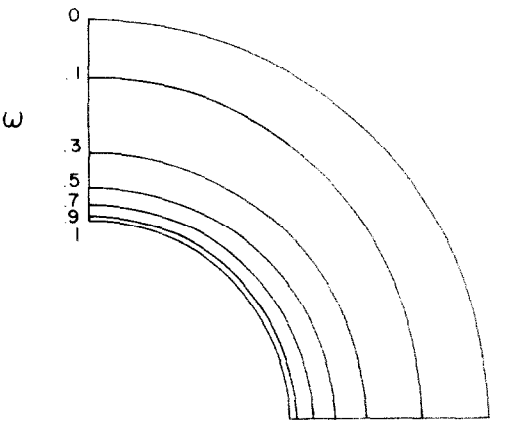

FIG. 13. The ω distribution for $\hat{\mu} = -1/3$, $Gr = 1 \times 10^5$.

The temperature distribution in this case is again similar to the conduction distribution. For $Gr = 0$ the differences in the two distributions are 4% of $(T_2 - T_1)$ near the north pole, and 7% of $(T_2 - T_1)$ near the equator. The region near the north pole contains fluid which is warmer than conduction temperatures, while near the equator the fluid is cooler. As the Grashof number increases, these differences also decrease, but at a slower rate than noted earlier. For example, for $Gr = 1 \times 10^5$, the temperature differences are 4% near the north pole (but over a smaller region) and 3% near the equator. The local wall heat flux for this configuration is shown in Fig. 14. The uppermost figure is for $Gr = 0$ and the lower figure is for $Gr = 1 \times 10^5$. The local heat flux values on the outer sphere clearly reflect the enhanced circulation of the clockwise eddy located near the outer sphere. The values along the inner sphere also demonstrate that this particular configuration is relatively unaffected by stable stratification.

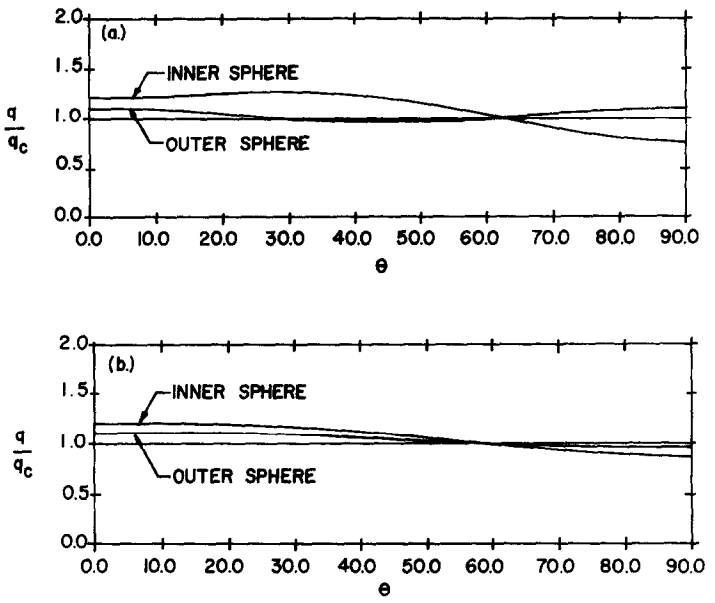

FIG. 14. Local heat flux for $\tilde{\mu} = -1/3$, (a) $Gr = 0$, (b) $Gr = 1 \times 10^5$.

(d) *Heat transfer*

The heat-transfer characteristics of all three configurations are summarized in Fig. 15. This plot shows the total heat flux across either sphere as a function of the Grashof number. The quantity $(Q/Q_c - 1)$ represents the fractional change in the total heat transfer over the rate calculated for conduction only. In the forced convection limit ($Gr = 0$) the value of $(Q/Q_c - 1)$ differs for each configuration according to the effectiveness of the secondary circulation. These values are 8.1×10^{-3}, 1.99×10^{-2}, and 1.85×10^{-2}, for $\tilde{\mu} = 0$, ∞, and $-1/3$ respectively [16]. Of most interest in this

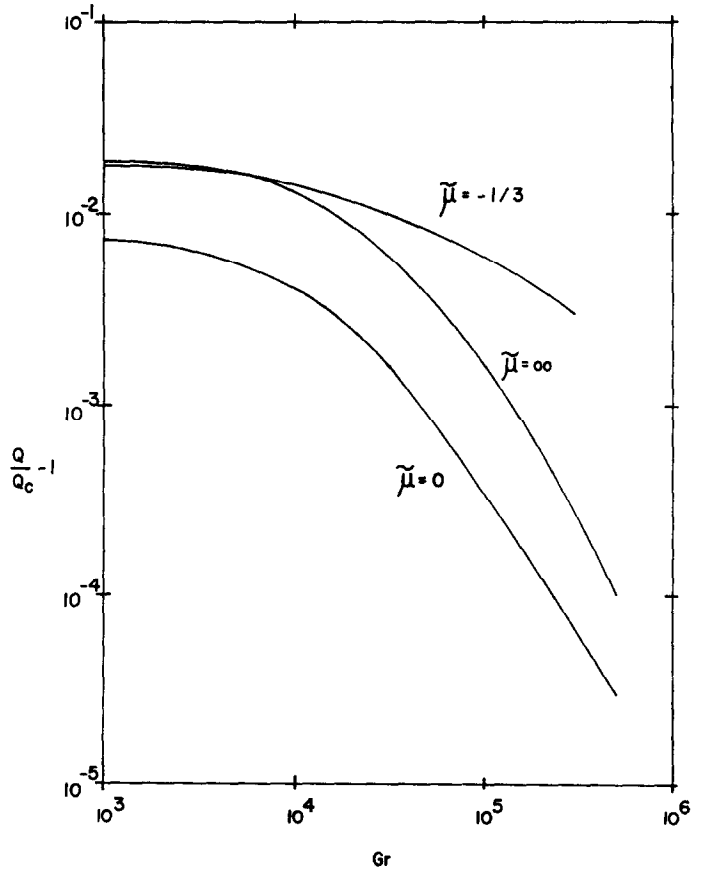

FIG. 15. Dependence of total heat flux on the Grashof number.

figure is the rate at which the total heat flux decreases with increasing Grashof number. The case of counter-rotating spheres ($\tilde{\mu} = -1/3$) shows significantly less rate of decrease in the heat-transfer rate than the other two configurations. This is not surprising in view of the resistance of this particular flow to the retarding action of the buoyancy forces.

4. SUMMARY

The effects of strong stable stratification on the steady laminar flow of a viscous fluid in a rotating spherical annulus have been investigated. Results are presented for three rotational configurations at a moderate rotation rate. The primary and secondary circulation patterns, the temperature distribution, and the heat-transfer characteristics of each flow are described. In all three cases, the buoyancy forces inhibit the circulation resulting from the differential rotation of the spheres, and reduce the overall heat transfer. For the case of a rotating inner sphere with the outer sphere at rest, the buoyancy forces generate a clockwise circulation near the outer sphere. The strength of this motion is comparable to that of the rotationally driven circulation for intermediate Grashof numbers. In the second configuration studied (inner sphere at rest, outer sphere rotating) the buoyancy forces retard the secondary circulation without distorting it to any great degree. The primary flow field described by the rotation ω is significantly distorted by buoyancy forces. As the Grashof number increases the rotation contours change near the equator. The cylindrical shear layer which exists at $Gr = 0$ is destroyed as the Grashof number increases. The last configuration studied (counter-rotating spheres) proved to be more resistant to the retarding influence of the buoyancy forces than the previous two cases. This is reflected in the relationship between the overall heat transfer and the Grashof number. The overall heat-transfer rate for the flow between counter-rotating spheres falls off less sharply with increasing Grashof number.

Acknowledgements—The support of National Science Foundation Grant ENG 75-18398 and the Engineering Research Center, University of Nebraska-Lincoln for this research has been appreciated.

REFERENCES

1. L. Howarth, Note on the boundary layer on a rotating sphere, *Phil. Mag.* **42**, 1308–15 (1951).
2. I. Proudman, The almost rigid rotation of viscous fluid between concentric spheres, *J. Fluid Mech.* **1**, 505–516 (1956).
3. H. P. Greenspan, On the transient motion of a contained rotating fluid, *J. Fluid Mech.* **21**, 673–696 (1964).
4. G. F. Carrier, Some effects of stratification and geometry in rotating fluids, *J. Fluid Mech.* **23**, 145–172 (1965).
5. C. E. Pearson, A numerical study of the time-dependent viscous flow between two rotating spheres, *J. Fluid Mech.* **28**, 323–336 (1967).
6. B. R. Munson and D. D. Joseph, Viscous incompressible flow between concentric rotating spheres. Part 1. Basic flow, *J. Fluid Mech.* **49**, 289–303 (1971).
7. B. R. Munson and D. D. Joseph, Viscous incompressible flow between concentric rotating spheres. Part 2. Hydrodynamic stability, *J. Fluid Mech.* **49**, 305–318 (1971).
8. V. Barcilon and J. Pedlosky, Lineary theory of rotating stratified fluid motions, *J. Fluid Mech.* **29**, 1–16 (1967).
9. V. Barcilon and J. Pedlosky, A unified linear theory of homogeneous and stratified rotating fluids, *J. Fluid Mech.* **29**, 609–621 (1967).
10. J. Pedlosky, Axially symmetric motion of a stratified rotating fluid in a spherical annulus of narrow gap, *J. Fluid Mech.* **36**, 401–415 (1969).
11. J. S. Allen, The effect of weak stratification and geometry on the steady motion of a contained rotating fluid, *J. Fluid Mech.* **43**, 129–144 (1970).
12. J. S. Allen, Upwelling of a stratified fluid in a rotating annulus: steady state. Part 1. Lineary theory, *J. Fluid Mech.* **56**, 429–445 (1972).
13. J. S. Allen, Upwelling of a stratified fluid in a rotating annulus: steady state. Part 2. Numerical solutions, *J. Fluid Mech.* **59**, 337–368 (1973).
14. R. W. Douglass, B. R. Munson and E. J. Shaughnessy, Combined convection in a rotating spherical annulus, *Int. J. Heat and Mass Transfer*, to be published.
15. E. J. Shaughnessy, J. R. Custer and R. W. Douglass, Partial spectral expansions for problems in thermal convection, *J. Heat Transfer*, to be published.
16. R. W. Douglass, Combined natural and forced thermal convection in a rotating spherical annulus. Ph.D. Dissertation, Dept. of Mechanical Engineering and Materials Science, Duke University (1975).

L'EFFET DE LA STRATIFICATION STABLE SUR LE MOUVEMENT DANS UN ESPACE ANNULAIRE SPHERIQUE TOURNANT

Résumé—On étudie les effets de la stratification stable sur l'écoulement permanent laminaire d'un fluide visqueux dans un espace annulaire sphérique tournant. Les configurations rotationnelles sont discutées: sphère interne tournant et sphère externe au repos; sphère interne fixe et sphère externe en rotation; et les deux sphères tournant en sens inverse. Les calculs concernent les circulations primaire et secondaire, la distribution des températures et les caractéristiques du transfert thermique. On montre que les forces de pesanteur sont sensibles par la réduction de l'intensité de la circulation secondaire et, dans un cas, elle provoque l'apparition d'une nouvelle configuration.

DER EINFLUSS STABILER SCHICHTUNG AUF DIE STRÖMUNG IN EINEM ROTIERENDEN SPHÄRISCHEN RINGRAUM

Zusammenfassung—Es wurdendie Wirkungen einer stabilen Schichtung auf die stationäre laminare Strömung eines viskosen Fluids in einem rotierenden sphärischen Ringraum untersucht. Drei Arten der Drehbewegung wurden behandelt: innere Kugel rotierend bei ruhender äußerer Kugel; innere Kugel ruhend

bei rotierender äußerer Kugel; und beide Kugeln in entgegengesetzter Richtung rotierend. Berechnet wurden die Primär- und Sekundärwirbel, die Temperatur-verteilung, die Wärmeübertragungseigenschaften der Strömung. Es stellte sich heraus, daß die Auftriebskräfte die Intensität der Sekundärwirbel abschwächen und in einem Fall ein neues Zirkulationsmuster hervorbrachten.

ВЛИЯНИЕ УСТОЙЧИВОЙ СТРАТИФИКАЦИИ НА ДВИЖЕНИЕ ЖИДКОСТИ ВО ВРАЩАЮЩЕМСЯ СФЕРИЧЕСКОМ КОЛЬЦЕВОМ КАНАЛЕ

Аннотация — В работе исследовано влияние устойчивой стратификации на стационарное ламинарное течение вязкой жидкости во вращающемся кольцевом канале. Рассмотрено три случая: внутренняя сфера вращается, наружная неподвижна; внутреняя сфера неподвижна, наружная вращается; обе сферы вращаются в противоположных направлениях. Проведен численный анализ первичных и вторичных течений, полей температур и теплообменных характеристик потока. Показано, что подъемные силы снижают интенсивность вторичной циркуляции, а в одном случае вызывают появление новой циркуляционной структуры.